Combinatorial Design of Copolymer Donor Materials for Bulk Heterojunction Solar Cells

Yongwoo Shin, Jaikai Liu, Joseph J. Quigley, IV, Heng Luo, and Xi Lin*

Department of Mechanical Engineering and Division of Materials Science and Engineering, Boston University, Boston, Massachusetts 02215, United States

ABSTRACT Seeking π-conjugated polymers with targeted optical band gaps is not only a grand scientific challenge but also in great practical need for systematically improving the performance of organic optoelectronic devices. This work presents a generic combinatorial band-gap design strategy over 780 different copolymer donor materials for bulk heterojunction solar cell applications. Predicted optical band gaps effectively cover the entire solar spectrum from infrared, to visible, to ultraviolet. Combined with empirical arguments widely acknowledged in the literature, the optimal copolymer structures are identified for both single and tandem cells with the optimal power conversion efficiencies.

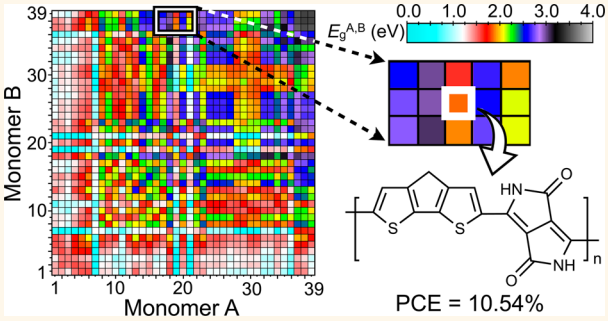

KEYWORDS: organic photovoltaic solar cells · bulk heterojunction · electron−phonon coupling · optical band gap · power conversion efficiency · materials design

In the past five years, the power conversion efficiency (PCE) of bulk heterojunction (BHJ) solar cells[1] has been doubled from 5% to slightly more than 10%. To a large extent, this was due to the introduction of low-band-gap copolymers.[2,3] These third-generation semiconducting polymers[4] typically contain two alternating π-conjugated monomer units of different electronegativities such that the more electronegative unit controls the lowest unoccupied molecular orbital (LUMO) of the copolymer, and the less electronegative unit controls the highest occupied molecular orbital (HOMO) of the copolymer. Using conjugated units of different electronegativities is an effective way to break the charge conjugation symmetry, thus separating the otherwise *conjugated* hole and electron states. The resulting band gaps of these copolymers[4] can reach well below typical band gaps of the conventional semiconducting polymers[5] such as polythiophene and may be tailored[6] to meet the optimal 1.3 eV in the detailed balance limit of any p−n junctions.[7]

On the basis of a set of simplified empirical arguments[8] consisting of a 0.3 eV minimal charge-transferring energy offset, an additional 0.3 eV energy offset between the built-in voltage and the actual open-circuit voltage, a typical 65% filling factor, and a typical 65% external quantum efficiency, Scharber *et al.* were able to set the PCE upper limit of 11% when donor materials of 1.2−1.8 eV band gaps are used together with [6−6]-phenyl-C_{61}-butyric acid methyl ester (PCBM) as the electron acceptor materials. Furthermore, Dennler *et al.*[3,9,10] followed similar arguments and suggested that tandem solar cells with a PCE of 15% may be achieved if donor materials with complementary band gaps of 1.6 and 1.3 eV were used. It is important to note that the PCE estimated based on these oversimplified empirical arguments may not necessarily be accurate.[11,12] Nevertheless, under these assumptions, complicated materials design of the PCE of BHJ solar cells can be reduced to a much simplified problem by tuning the optical band gaps of donor materials and aligning their LUMO energy levels relative to the LUMO levels of their corresponding acceptors.

Designing optical band gaps of optoelectroactive materials, however, is not a straightforward task since it requires knowledge of the two-particle Green's function propagator.[13] As one of the most successful quantum

* Address correspondence to linx@bu.edu.

Received for review March 11, 2014 and accepted May 14, 2014.

Published online 10.1021/nn5014066

many-body theories, the first-principles density functional theory (DFT) guarantees only the ground-state properties.[14] In practice, the convex nature of all the existing energy functionals that are based on the local density approximation inevitably favors the fractional charge states[15] with delocalized electronic wave functions in several strongly correlated materials systems.[16] One of these difficult cases concerns the self-localized soliton and polaron states in π-conjugated polymers,[5] for which even the time-dependent DFT[17] (TDDFT) under the adiabatic local density approximation is known to fail in the extended polymer limit.[18] To resolve this strong-correlation problem in π-conjugated systems, we have recently been developing an accurate, transferrable, and computationally efficient model Hamiltonian, the adapted Su–Schrieffer–Heeger (aSSH) Hamiltonian,[6,19–21] which renormalizes the many-electron correlation into a universal electron–phonon coupling constant.[5,19,22]

The aSSH Hamiltonian is built upon two fundamental assumptions: separability of π-electrons from σ-electrons and equality in the electron–phonon coupling among all π-electrons. First, we assume that low-energy excitations near the Fermi surface of π-conjugated systems can be faithfully captured by the wave functions of π-electrons, such that those energetically much stronger σ-bonds are inherent Harmonic oscillators whose role is to hold the chemically bonded π-conjugated units together. On the basis of such energy differences between the π- and σ-bands, the excitation of π-electrons near the Fermi surface can be coupled to the rigid σ-phonons, and through the Schrieffer–Wolff transformation[23] they can get self-trapped when coupled to two σ-phonons with the opposite wave-vectors. Similar to the Cooper pair instability,[23] we expect the existence of weakly interacting σ-phonon-coupled quasi-π-electrons that can precisely reproduce the low-energy excitations near the Fermi level as guaranteed by the Landau–Fermi liquid theory. In other words, the separability assumption between π- and σ-electrons essentially implies the possibility of renormalizing the strongly interacting π-electrons into weakly interacting σ-phonon-screened quasi-π-electrons for relevant low-energy excitation processes occurring in these π-conjugated systems. In conducting polymers, for example, screening of π-electrons by the quasi-one-dimensional (1D) optical phonons leads to the Peierls instability[24,25] and formation of self-localized topological soliton and polaron gap states.[5]

Second, we assume that all π-electrons are screened by σ-phonons in exactly the same manner, regardless of their chemical origins. Explicitly, we assume that the electron–phonon coupling strength λ[5,26] is a universal constant applicable to all kinds of π-electrons, on the C, N, O, and S atomic sites, in six- and five-membered conjugated rings, and in linear chains, branching dendrimers, two-dimensional graphene, and fullerene structures with twelve disclinations. Physically, such a dimensionless constant λ specifies the coupling strength of a Dirac fermion (electron) to a continuum boson (phonon) field[27] as described by the Gross–Neven model field[28] in the semiclassical limit.[29] For simplicity and also for practical reasons, here we choose the original SSH value of $\lambda = 0.20$, which corresponds to an optical band gap of 1.3 eV for *trans*-polyacetylene.[5,19] The validity and consequence of fixing such a constant λ value certainly deserve systematic and more thorough investigations. Nevertheless, in a recent comprehensive survey,[6] Botelho *et al.* found it predicts reasonably accurate optical band-gap values for nearly 200 independent π-conjugated systems whose optical spectra are available in the literature. A systematically underestimated error of 0.05 eV with a standard deviation of 0.16 eV was found against the corresponding experimental measurements.[6] Figures S1a and S1b of the Supporting Information summarize these direct comparisons for the second- and third-generation conjugated polymers, respectively. As shown in Figure S2a, accuracy in the predicted aSSH optical band-gap values (black crosses) far exceeds the conventional Hartree–Fock (HF, yellow circles), DFT (blue triangles), and TDDFT (red circles) results. Moreover, based on the universal electron–phonon coupling assumption for all π-electrons, Shin and Lin were able to incorporate three-dimensional (3D) interchain π–π interactions *via* exponentially decaying hopping integrals[21] and obtained accurate optical adsorption spectra over the entire experimentally relevant energy ranges for several representative second-generation (Figure S1c) and third-generation (Figure S1d) conjugated polymers. They were also able to probe the photoinduced charge transfer processes across the BHJ interfaces.[21]

Going beyond the aSSH quasi-particle picture as described above, one may construct the Peierls–Hubbard Hamiltonians,[25,29,30] which explicitly take electron correlations and higher-order electron–phonon coupling effects into account. These correlation terms are crucial to probe the negative spin-density waves,[31] multiple gap states,[30] 3D conformation couplings,[32,33] and a few other intriguing phenomena.[5] Finally, we note that the quantum nature of carbon and other heteroatoms would also be important in probing real-time dynamics when two adiabatic potential energy surfaces cross each other.[34,35] Since this work was focused primarily on designing the copolymer band gaps and their LUMO level alignments with acceptors, both the explicit electron correlations and nonadiabatic quantum dynamics effects were neglected.

RESULTS AND DISCUSSION

The aSSH Hamiltonian[6,19–21] is implemented in this work to perform the combinatorial design of copolymer materials for both single and tandem BHJ solar cells. A set of 39 commonly used π-conjugated

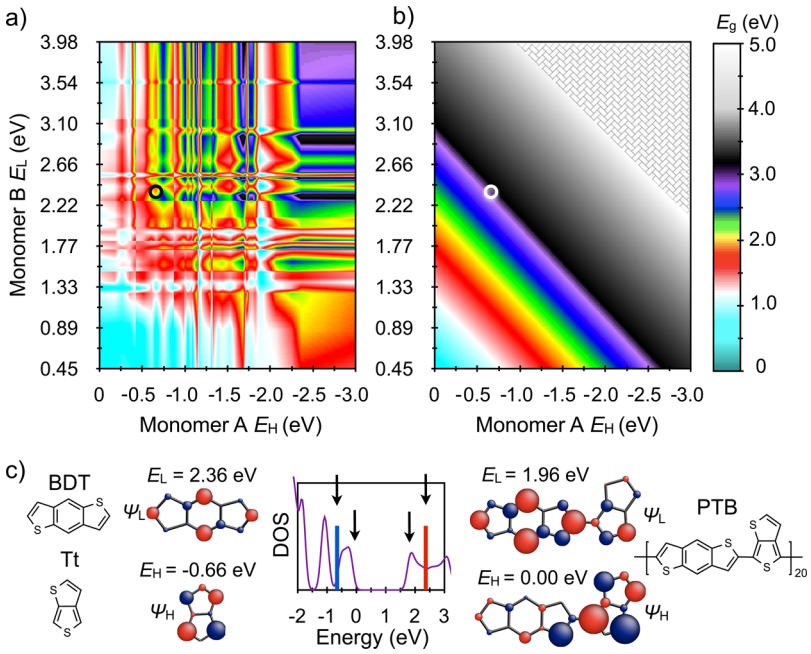

Figure 1. (a) Predicted copolymer band gap ($E_g^{A,B}$) by the aSSH Hamiltonian as a function of the HOMO energy (E_H) of monomer A (refer to Figure S3) and the LUMO energy (E_L) of monomer B (refer to Figure S4). All of the $E_g^{A,B}$ values are color-coded according to the corresponding photon energies: true colors for visible light between 1.65 and 3.27 eV, cyan to white for infrared, and black to gray for ultraviolet ranges. All (A−B) copolymers contain 20 repeating (A−B) units, representing the long-polymer limit. The aSSH $E_g^{A,B}$ values shown in (a) differ significantly from the simple difference between the lower E_L and higher E_H of the two monomer units, which is shown in (b). (c) The energy difference between E_L of monomer BDT and E_H of monomer Tt is 3.02 eV, much larger than the copolymer PTB band gap of 1.96 eV. The HOMO and LUMO wave functions of PTB show clear hybridization characteristics among alternating monomer units.

monomers are chosen as the building blocks, listed in Figure S3 in descending order according to their HOMO energies (E_H) and similarly listed in Figure S4 according to their LUMO energies (E_L) ascendingly. The complete combination gives a total of 780 independent polymers, including 741 (A−B) copolymers in which the A and B units are different and 39 regular polymers. Marking the sorted monomer E_H and E_L on the *x*-axis and *y*-axis, respectively, we plot in Figure 1a our computed aSSH band gap ($E_g^{A,B}$) for all 780 copolymers. The $E_g^{A,B}$ values are color-coded according to their corresponding photon energies for light and represented as red to purple for visible, cyan to white for infrared, and black to gray for ultraviolet ranges.

Intuitively, one might expect that the $E_g^{A,B}$ value of a given (A−B) copolymer could simply be the difference in energy between the higher E_H and lower E_L of two individual A and B monomers. Such a straightforward energy difference is plotted in Figure 1b using the same color scheme as Figure 1a. Comparing the simple stripe patten of Figure 1b to the aSSH results of Figure 1a, one easily observes that the optical band gap of a (A−B) copolymer cannot be predicted based only on the HOMO and LUMO levels of two separate monomers. Instead, full diagonalization of the aSSH Hamiltonian was utilized to obtain the phonon-screened quasi-particle energies.

Consider one popular copolymer (PTB) as an illustrative example, whose monomer constituents are thieno[3,4-*b*]thiophene (Tt) and benzo[1,2-*b*:4,5-*b*′]-dithiophene (BDT). Their chemical structures, density of states (DOS), and frontier orbital wave functions are shown in Figure 1c. Using a series of PTB-based donor materials with different side groups, one of the highest single-cell PCE of 8% was recently reported.[36] Presented in Figure 1c, the energy difference between E_L of BDT and E_H of Tt is 3.02 eV, shown as the ultraviolet region (Figure 1b, white circle), is much larger than the PTB band gap of 1.96 eV computed by the aSSH Hamiltonian (Figure 1a, black circle). The delocalized HOMO and LUMO wave functions of PTB (Figure 1c) over both the Tt and DBT units are clear indications of strong hybridization effects among the frontier orbitals of both monomer units.

Since the copolymer optical band gaps are not directly related to the HOMO and LUMO energy values of individual monomers, we may replot the aSSH $E_g^{A,B}$ data of Figure 1a along different *x*- and *y*-axes. From the materials design aspect, it is often important to quantify how much the copolymer band gap $E_g^{A,B}$ may vary when one particular monomer A is copolymerized with another random monomer B. Mathematically, we can define the energy dispersion width *w* of a particular monomer A as

$$w^A = \mathrm{Max}(E_g^{A,B}, \forall B) - \mathrm{Min}(E_g^{A,B}, \forall B)$$

where monomer B runs through all 39 monomer units considered in this materials design study. The

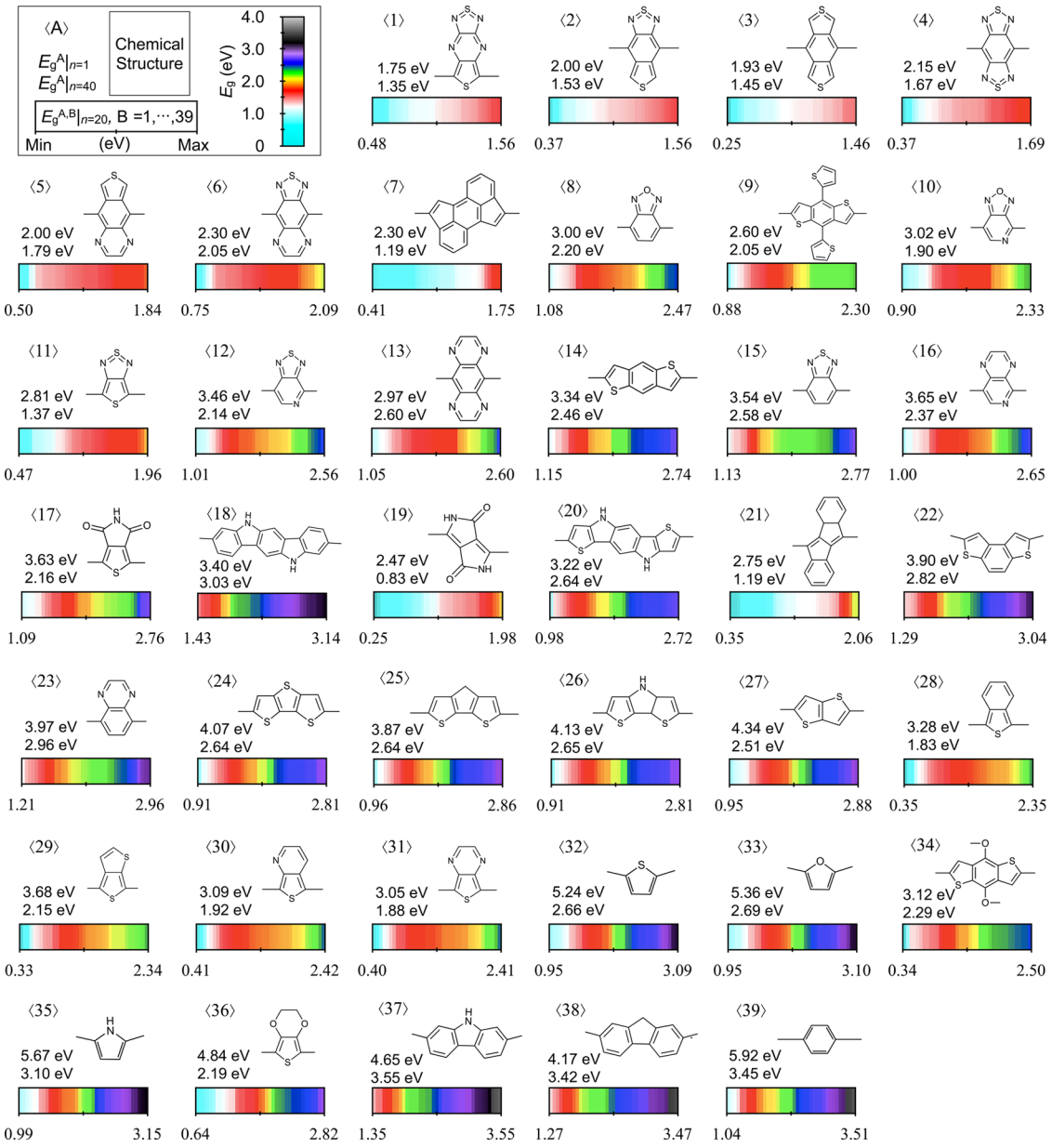

Figure 2. Tabulated copolymer band-gap dispersivity map for each monomer unit in the order of their energy dispersion widths *w* from the smallest to largest values. For each monomer unit ⟨A⟩, the map shows the monomer chemical structure, monomer band gap ($E_g^A|_{n=1}$), polymer band gap ($E_g^A|_{n=40}$), and all 39 copolymer bandgaps $\{E_g^{A,B}|_{n=20}, \forall B\}$. Here *n* specifies the length of the repeating units used in the aSSH Hamiltonian calculation. Copolymer band gaps $E_g^{A,B}$ are color-coded according to the corresponding photon energies as in Figure 1. Each color-coded $E_g^{A,B}$ bar consists of 39 small color-coded segments of identical segment width, representing all 39 copolymer combinations.

complete list of the copolymer $\{E_g^{A,B}, \forall B\}$ is tabulated in Figure 2 for every monomer, labeled ascendingly in the order of their energy dispersion width *w* values.

As the legend indicates, Figure 2 collects in a graphical survey a few key *design indices* for every single monomer unit, including the chemical structure, monomer band gap, polymer band gap, and all 39 copolymer band gaps. These copolymer band gaps $E_g^{A,B}$ are color-coded using the same coloring scheme as Figure 1a, and they are plotted together one-by-one and side-by-side with the same segment width. Namely, along each colored $E_g^{A,B}$ bar shown in Figure 2 there are 39 small colored segments, one-by-one from the lowest value on the left to the largest value on the right. Therefore, for each monomer A, colors with relatively large widths generally imply that their corresponding $E_g^{A,B}$ values are dominant among all the possible choices of monomer B.

For example, band gaps of those copolymers that have monomer ⟨5⟩ as one constituent unit predominantly fall into the red-light energy range. Monomer ⟨7⟩ is one excellent monomer constituent if one seeks copolymers with band gaps in the infrared region. While $\{E_g^{1,B}, \forall B\}$ has the narrowest energy dispersivity

covering mainly the infrared and red-light region, $\{E_g^{18,B}, \forall B\}$ can effectively reproduce all the colors in the visible-light spectrum but nothing else. As shown in Figure 2, rich dispersivity and complicity in the copolymer $E_g^{A,B}$ values are clear indications that there are no simple correlations between the monomer band gaps and their corresponding copolymer band gaps. In this sense, Figure 2 may be regarded as basic guiding principles beyond simple chemical intuitions to design new copolymers for the BHJ solar cells.

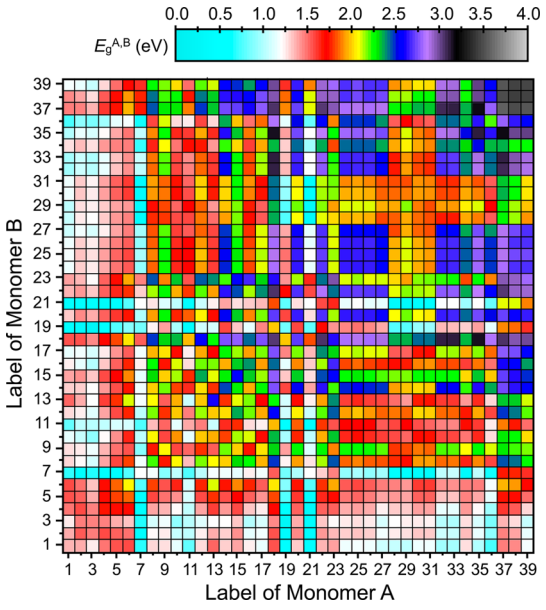

Figure 3. Color-coded copolymer band-gap $E_g^{A,B}$ map as a function of the two constituent monomer energy dispersivity labels defined in Figure 2. Note that this band-gap map contains information that is identical to that in Figure 1a, but it is plotted from the materials design perspective.

Combining these individual pieces of information, we replot in Figure 3 the color-coded $E_g^{A,B}$ along the ordered *x*- and *y*-axes according to the energy dispersivity label defined in Figure 2. In this symmetric band-gap figure, copolymer PTB is located at (*x*,*y*) = (14,29) or (29,14) as an orange-yellow square, which corresponds to the band gap $E_g^{14,29}$ = 1.96 eV. Compared to the apparently intuitive, but indeed misleading, ordered HOMO and LUMO energy axes in Figure 1, the new energy dispersivity labels of Figure 3 lay out a valuable *treasure map, vis-à-vis design space map*, for one to look up novel copolymer structures with their targeted optical band gaps. There are plenty of candidate copolymer combinations for all the optical band-gap energy values ranging from infrared as low as 0.41 eV to ultraviolet as high as 3.55 eV using only these 39 monomer building blocks. The abundant red and infrared squares in Figure 3 indicate that these conjugated

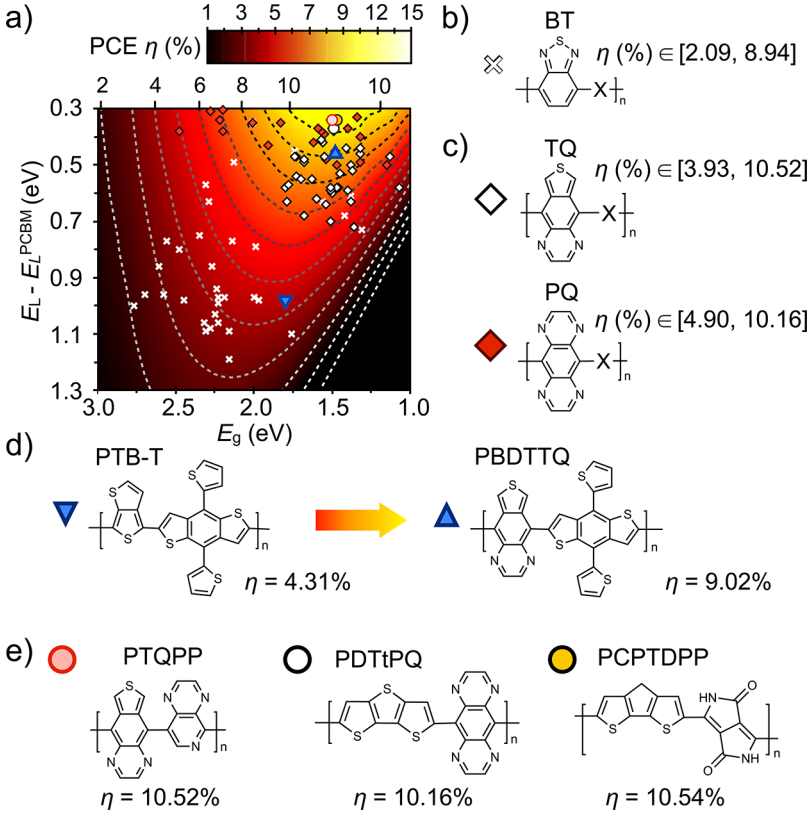

Figure 4. (a) Single-cell PCE η as a function of the donor band gap (E_g) and the donor LUMO energy offset with respect to PCBM, $E_L - E_L^{PCBM}$. We regenerate this plot based on the assumptions described in ref 8. Copolymers with BT (white crosses) as one constituent generally have lower PCE as compared to TQ (white diamonds) and PQ (red diamonds). (d) On replacing Tt in PTB-T (blue triangle pointing downward) by TQ to form PBDTTQ, the PCE increases from 4.3% to 9.0%. (e) Three copolymer structures with predicted η > 10% are PTQPP (pink circle), PDTtPQ (white circle), and PCPTDPP (orange circle).

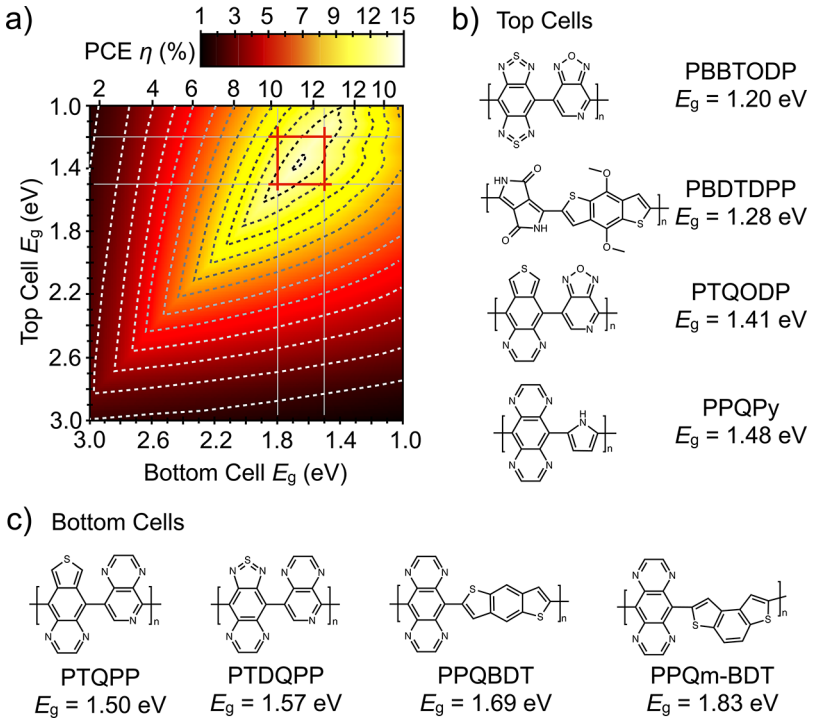

Figure 5. (a) Tandem-cell PCE η as a function of the top-cell donor band gap (E_g^T) and the bottom-cell donor band gap (E_g^B), both using PCBM as the electron acceptors. We regenerate this plot based on the assumptions described in ref 9. The optimal tandem-cell PCEs η > 12% require very narrow energy windows for both $E_g^T \in$ (1.20,1.50) eV and $E_g^B \in$ (1.50,1.80) eV (annotated with red box). A list of the optimal copolymer donors for the top cell (b) and bottom cell (c).

copolymers, third-generation conducting polymers, are truly complementary to the second-generation conducting polymers that have systematically larger band gaps. Refer to Figure S1 for detailed comparisons. Furthermore, by introducing functional side-group modifications[37,38] to improve their solubility and morphology, we expect the copolymer combination results shown in Figures 2 and 3 might lead to potential paradigm shifts in the BHJ solar cell materials design from conventional trial-and-error approaches to potentially more efficient physics-based design guidelines.

Following the empirical assumptions introduced by Scharber *et al.*,[8,10] we may apply our new copolymer structure−band-gap guidelines to directly improve the PCE of existing single-cell and tandem-cell devices. For example, the widely used monomer benzo[*c*]-[1,2,5]thiadiazole (BT, Figure 4b) is not necessarily one of the best copolymer constituents, since its copolymer PCE values scatter between 2.1% and 8.9% (Figure 4a, white crosses) when copolymerized with those 39 monomer units. As implied by the empirical assumptions,[8,10] these predicted PCE values may be regarded as the PCE upper bounds of existing BHJ devices using the BT-based copolymers,[39−45] where the reported PCE value range is from 0.8% to 6.4%.

On the other hand, Figure 4a indicates that thieno-[3,4-*g*]quinoxaline (TQ) and pyrazino[2,3-*g*]quinoxaline (PQ) are much better monomer choices, since their copolymer PCEs are clustered around 8% (white and red diamonds, respectively), largely independent of the other monomer constituents. In particular, if one replaces the monomer Tt unit in copolymer PBT-T by the TQ monomer unit (Figure 4d), the PCE would increase from 4.3% for PTB-T (Figure 4a, blue triangle pointing downward) to 9.0% for PBDTTQ (Figure 4a, blue triangle pointing upward). Among all 780 copolymer combinations considered in this work, Figure 4a suggests that the highest PCE values may be achieved by using poly-TQ-pyrido[3,4-*b*]pyridine (PTQPP; pink circle), whose energy dispersivity coordinates shown in Figure 3 are (5,16), poly dithieno[3,2-*b*:2′,3′-d]thiophene-PQ (PDTtPQ; white circle) located at (13,24) in Figure 3, and poly cyclopentadithiophene-diketopyrrolopyrrole (DPP) (PCPTDPP; orange circle) located at (19,38) in Figure 3.

To reach beyond the 11% PCE limit as shown in Figure 4a, Dennler *et al.*[9] proposed to build various tandem-cell structures.[10] Following their arguments, we plot in Figure 5a the tandem-cell PCE values as a function of the donor band gaps of the top cell, E_g^T, and the bottom cell, E_g^B. Figure 5a is obtained by reducing the remaining materials variables, such as their LUMO energy levels, external quantum efficiencies, and internal quantum efficiency,[9] for the optimal PCE values.

Under these assumptions,[9] we can also apply our predicted band-gap design map (Figure 3) to create a list of optimal copolymer materials. These optimal copolymer structures are located in the annotated red box (η > 12%) of Figure 5a, with their corresponding

$E_g^T \in$ (1.20,1.50) eV and $E_g^B \in$ (1.50,1.80) eV. Figure 5b gives an explicit list of the top-cell copolymers, including poly benzo[1,2-*c*;3,4-*c*']bis[1,2,5]thiadiazole-[1,2,5]-oxadiazolo[3,4-*c*]pyridine (PBBTODP), poly-BDT-2,5-dihydropyrrolo[3,4-*c*]pyrrole-1,4-dione (PBDTDPP), TQODP, and poly-PQ-pyrrole (PPQPy). Similarly, Figure 5c lists the optimal copolymers for the bottom cell, including PTQPP, poly-[1,2,5]thiadiazolo[3,4-*g*]quinoxaline-PP (PTDQPP), PPQBDT, and poly-PPQ-m-BDT (PPPQm-BDT). Among them, the top-cell PTQODP and bottom-cell PPQBDT combination gives the highest value of PCE, η = 14.1%. It is important to note that since all the optimal copolymer structures shown in Figures 4 and 5 have their LUMO energy (E_L) aligned relative to E_L^{PCBM}, one needs to use the *treasure map* of Figure 3 and LUMO energy level appropriate materials in Figure S4 to reselect new copolymer structures of other candidate electron acceptor materials for organic solar cells.

CONCLUSION

In summary, we present in this work the first combinatorial design over 780 different π-conjugated copolymer donor materials for the BHJ solar cell application. A comprehensive structure−band-gap design map is generated and color-coded using their corresponding photon absorption energies. When combining such a structure−band-gap design map with a few widely acknowledged empirical arguments in the literature, we can directly link the copolymer structures to the overall PCE for both the single-cell and tandem-cell devices. Despite the need to further unentangle these simplified empirical arguments into a much more complicated electron−phonon dynamics and multiphase-morphology formation and evolution; the capability of accurately predicting the optical band gaps of nontrivial copolymer structures is nevertheless one significant step toward the predictive materials design of π-conjugated structures.

METHODS

All the optical band-gap calculations presented in this work are performed using the aSSH Hamiltonian.[6,19−21] Refer to the Supporting Information for more details. All the chemical structures were drawn using ChemBioDraw, and wave functions were plotted using AtomEye.[46]

Conflict of Interest: The authors declare no competing financial interest.

Supporting Information Available: Detailed compuatational methods, benchmark data of the second- and third-generation polymers, comparison with other electronic structure methods, and HOMO and LUMO energies of monomer units. This material is available free of charge *via* the Internet at http://pubs.acs.org.

REFERENCES AND NOTES

1. Yu, G.; Gao, J.; Hummelen, J. C.; Wudl, F.; Heeger, A. J. Polymer Photovoltaic Cells: Enhanced Efficiencies *via* a Network of Internal Donor-Acceptor Heterojunctions. *Science* **1995**, *270*, 1789–1791.
2. Liang, Y.; Yu, L. A New Class of Semiconducting Polymers for Bulk Heterojunction Solar Cells with Exceptionally High Performance. *Acc. Chem. Res.* **2010**, *43*, 1227–1236.
3. Ameri, T.; Li, N.; Brabec, C. J. Highly Efficient Organic Tandem Solar Cells: A Follow Up Review. *Energy Environ. Sci.* **2013**, *6*, 2390–2413.
4. Heeger, A. J. Semiconducting Polymers: The Third Generation. *Chem. Soc. Rev.* **2010**, *39*, 2354.
5. Heeger, A. J.; Kivelson, S.; Schrieffer, J. R.; Su, W. P. Solitons in Conducting Polymers. *Rev. Mod. Phys.* **1988**, *60*, 781–850.
6. Botelho, A. L.; Shin, Y.; Liu, J.; Lin, X. Structure and Optical Bandgap Relationship of π-Conjugated Systems. *PLoS One* **2014**, *9*, e86370.
7. Shockley, W.; Queisser, H. J. Detailed Balance Limit of Efficiency of p-n Junction Solar Cells. *J. Appl. Phys.* **1961**, *32*, 510–519.
8. Scharber, M. C.; Mühlbacher, D.; Koppe, M.; Denk, P.; Waldauf, C.; Heeger, A. J.; Brabec, C. J. Design Rules for Donors in Bulk-Heterojunction Solar Cells—Towards 10% Energy-Conversion Efficiency. *Adv. Mater.* **2006**, *18*, 789–794.
9. Dennler, G.; Scharber, M. C.; Ameri, T.; Denk, P.; Forberich, K.; Waldauf, C.; Brabec, C. J. Design Rules for Donors in Bulk-Heterojunction Tandem Solar Cells Towards 15% Energy-Conversion Efficiency. *Adv. Mater.* **2008**, *20*, 579–583.
10. Ameri, T.; Dennler, G.; Lungenschmied; Brabec, C. J. Organic Tandem Solar Cells: A Review. *Energy Environ. Sci.* **2009**, *2*, 347–363.
11. Blouin, N.; Michaud, A.; Gendron, D.; Wakim, S.; Blair, E.; Neagu-Plesu, R.; Belletête, M.; Durocher, G.; Tao, Y.; Leclerc, M. Toward a Rational Design of Poly(2,7-carbazole) Derivatives for Solar Cells. *J. Am. Chem. Soc.* **2008**, *130*, 732–742.
12. Price, S. C.; Stuart, A. C.; Yang, L.; Zhou, H.; You, W. Fluorine Substituted Conjugated Polymer of Medium Band Gap Yields 7% Efficiency in Polymer-Fullerene Solar Cells. *J. Am. Chem. Soc.* **2011**, *133*, 4625–4631.
13. Mattuck, R. D. *A Guide to Feynman Diagrams in the Many-Body Problem*, 2nd ed.; McGraw-Hill: New York, 1976.
14. Hohenberg, P.; Kohn, W. Inhomogeneous Electron Gas. *Phys. Rev.* **1964**, *136*, B864–B871.
15. Parr, R. G.; Yang, W. *Density-Functional Theory of Atoms and Molecules*; The International Series of Monographs on Chemistry; Oxford University: New York, 1989.
16. Cohen, A. J.; Mori-Sanchez, P.; Yang, W. Insights into Current Limitations of Density Functional Theory. *Science* **2008**, *321*, 792–794.
17. Runge, E.; Gross, E. K. U. Density-Functional Theory for Time-Dependent Systems. *Phys. Rev. Lett.* **1984**, *52*, 997–1000.
18. van Faassen, M.; de Boeij, P. L.; van Leeuwen, R.; Berger, J. A.; Snijders, J. G. Ultranolocality in Time-Dependent Current-Density-Functional Theory: Application to Conjugated Polymers. *Phys. Rev. Lett.* **2002**, *88*, 186401.
19. Li, M.; Lin, X. Adapted Su-Schrieffer-Heeger Hamiltonian for Polypyrrole. *Phys. Rev. B* **2010**, *82*, 155141.
20. Botelho, A. L.; Shin, Y.; Li, M.; Jiang, L.; Lin, X. Unified Hamiltonian for Conducting Polymers. *J. Phys.: Condens. Matter* **2011**, *23*, 455501.
21. Shin, Y.; Lin, X. Modeling Photoinduced Charge Transfer Across π-Conjugated Heterojunctions. *J. Phys. Chem. C* **2013**, *117*, 12432–12437.
22. Su, W.; Schrieffer, J.; Heeger, A. Solitons in Polyacetylene. *Phys. Rev. Lett.* **1979**, *42*, 1698–1701.
23. Phillips, P. *Advanced Solid State Physics*; Westview Press: Boulder, 2003.
24. Peierls, R. E. *Quantum Theory of Solids*; The International Series of Monographs on Physics; Oxford University Press: New York, 1955.
25. Li, M.; Lin, X. Twin Distortion of the Peierls Instability. *Pays. Rev. B* **2010**, *81*, 153102.

26. Conwell, E. Transport in Trans-Polyacetylene. *IEEE EEE Trans. Electr. Insul.* **1987**, 591–627.
27. Takayama, H.; Lin-Liu, Y. R.; Maki, K. Continuum Model for Solitons in Polyacetylene. *Phys. Rev. B* **1980**, *21*, 2388–2393.
28. Gross, D. J.; Neveu, A. Dynamical Symmetry Breaking in Asymptotically Free Field Theories. *Phys. Rev. D* **1974**, *10*, 3235–3253.
29. Campbell, D. K. Conducting Polymers and Relativistic Field Theories. *Synth. Met.* **2002**, *125*, 117.
30. Lin, X.; Föerst, C.; Li, J.; Yip, S. Multiple Self-Localized Electronic States in Trans-Polyacetylene. *Proc. Nat. Acad. Sci. U.S.A* **2006**, *103*, 8943–8946.
31. Subbaswamy, K. R.; Grabowski, M. Bond Alternation, On-Site Coulomb Correlations, and Solitons in Polyacetylene. *Phys. Rev. B* **1981**, *24*, 2168–2173.
32. Lin, X.; Li, J.; Yip, S. Controlling Bending and Twisting of Conjugated Polymers *via* Solitons. *Phys. Rev. Lett.* **2005**, *95*, 198303.
33. Lin, X.; Li, J.; Smela, E.; Yip, S. Polaron-Induced Conformation Change of a Single Polypyrrole Chain: An Intrinsic Actuation Mechanism. *Int. J. Quantum Chem.* **2005**, *102*, 980–985.
34. Tully, J. C. Molecular Dynamics with Electronic Transitions. *J. Chem. Phys.* **1990**, *93*, 1061–1071.
35. Tully, J. C. Perspective: Nonadiabatic Dynamics Theory. *J. Chem. Phys.* **2012**, *137*, 22A301.
36. Liang, Y.; Wu, Y.; Feng, D.; Tsai, S.-T.; Son, H.-J.; Li, G.; Yu, L. Development of New Semiconducting Polymers for High Performance Solar Cells. *J. Am. Chem. Soc.* **2009**, *131*, 56–57.
37. Yiu, A. T.; Beaujuge, P. M.; Lee, O. P.; Woo, C. H.; Toney, M. F.; Fréchet, J. M. J. Side-Chain Tunability of Furan-Containing Low-Band-Gap Polymers Provides Control of Structural Order in Efficient Solar Cells. *J. Am. Chem. Soc.* **2012**, *134*, 2180–2185.
38. Balakrishnan, K.; Datar, A.; Naddo, T.; Huang, J.; Oitker, R.; Yen, M.; Zhao, J.; Zang, L. Effect of Side-Chain Substituents on Self-Assembly of Perylene Diimide Molecules: Morphology Control. *J. Am. Chem. Soc.* **2006**, *128*, 7390–7398.
39. Donaghey, J. E.; *et al.* Pyrroloindacenodithiophene Containing Polymers for Organic Field Effect Transistors and Organic Photovoltaics. *J. Mater. Chem.* **2011**, *21*, 18744–18752.
40. Yue, W.; Zhao, Y.; Shao, S.; Tian, H.; Xie, Z.; Geng, Y.; Wang, F. Novel NIR-Absorbing Conjugated Polymers for Efficient Polymer Solar Cells: Effect of Alkyl Chain Length on Device Performance. *J. Mater. Chem.* **2009**, *19*, 2199–2206.
41. Svensson, M.; Zhang, F.; Veenstra, S.; Verhees, W.; Hummelen, J.; Kroon, J.; Inganäs, O.; Andersson, M. High-Performance Polymer Solar Cells of an Alternating Polyfluorene Copolymer and a Fullerene Derivative. *Adv. Mater.* **2003**, *15*, 988–991.
42. Zhu, Z.; Waller, D.; Gaudiana, R.; Morana, M.; Muhlbacher, D.; Scharber, M.; Brabec, C. Panchromatic Conjugated Polymers Containing Alternating Donor/Acceptor Units for Photovoltaic Applications. *Macromolecules* **2007**, *40*, 1981–1986.
43. Blouin, N.; Michaud, A.; Leclerc, M. A Low-Bandgap Poly-(2,7-Carbazole) Derivative for Use in High-Performance Solar Cells. *Adv. Mater.* **2007**, *19*, 2295–2300.
44. Huo, L.; Hou, J.; Zhang, S.; Chen, H.-Y.; Yang, Y. A Polybenzo[1,2-b:4,5-b′]dithiophene Derivative with Deep HOMO Level and Its Application in High-Performance Polymer Solar Cells. *Angew. Chem., Int. Ed.* **2010**, *49*, 1500–1503.
45. Chen, Y. C.; Yu, C. Y.; Fan, Y. L.; Hung, L. I.; Chen, C. P.; Ting, C. Low-Bandgap Conjugated Polymer for High Efficient Photovoltaic Applications. *Chem. Commun.* **2010**, *46*, 6503–6505.
46. Li, J. AtomEye: An Efficient Atomistic Configuration Viewer. *Modell. Simul. Mater. Sci. Eng.* **2003**, *11*, 173.